

# Kuramoto model based analysis reveals oxytocin effects on brain network dynamics

Shuhan Zheng<sup>1</sup>, Zhichao Liang<sup>1</sup>, Youzhi Qu<sup>1</sup>,  
Qingyuan Wu<sup>3</sup>, Haiyan Wu<sup>2,\*</sup>, Quanying Liu<sup>1,\*</sup>

March 6, 2022

<sup>1</sup> Shenzhen Key Laboratory of Smart Healthcare Engineering,  
Southern University of Science and Technology, Shenzhen 518005, China  
<sup>2</sup> Centre for Cognitive and Brain Sciences and Department of Psychology,  
University of Macau, Macau, China

<sup>3</sup> State Key Laboratory of Cognitive Neuroscience and Learning &  
IDG/McGovern Institute for Brain Research, Beijing Normal University,  
Beijing 100875, China

\* Corresponding to haiyanwu@um.edu.mo (H.W); liuqy@sustech.edu.cn (Q.L)

## Abstract

The oxytocin effects on large-scale brain networks such as Default Mode Network (DMN) and Frontoparietal Network (FPN) have been largely studied using fMRI data. However, those studies are mainly based on the statistical correlation or bayesian causality inference, lacking physical and neuroscience level interpretability. Here, we propose a Kuramoto model physical-based framework to investigate oxytocin effects on the phase dynamical neural coupling in DMN and FPN. Tested on fMRI data from 59 participants administrated with either oxytocin or placebo, we demonstrate that oxytocin changes the topology of brain communities in DMN and FPN, leading to higher synchronization in the DMN and lower synchronization in the FPN, as well as a higher variance of the coupling strength within the DMN and more flexible coupling patterns across time. These results together imply that oxytocin may increase the capability to overcome the dispersion of corresponding intrinsic oscillations and yield flexibility in neural synchrony under various social contexts, providing new evidence to account for oxytocin modulated social behaviors. Our proposed Kuramoto model-based framework can be a potential tool in network neuroscience and offers physical and neural insights into phase dynamics in the brain.

keywords: Oxytocin Effects; Default Mode Network; Frontoparietal Network; fMRI; Kuramoto Model.

# 1 Introduction

Brain is a complex network with spatially distributed but temporally synchronized regions [1, 30, 55]. The conventional methods to characterize synchronization between brain regions are mostly based on statistical properties of time series, such as Pearson correlation [51], phase coherence [11] and Granger causality [39]. Kuramoto model, initially proposed by Japanese physicist Yoshiki Kuramoto, is a phase dynamics model to characterize the phase coupling of oscillators [27]. In contrast to statistic-based methods, synchronization in the Kuramoto model can explain more physical phenomena, which is quantified by the estimated model parameters. Kuramoto model has been extensively applied to complex network analysis, ranging from chemical networks [28] to biological networks [3].

Recently, the Kuramoto model has been brought into network neuroscience for revealing neural synchronization across brain regions [6, 23, 42]. Synchronization of neural dynamics has been applied to elucidate the existence of the hierarchical modular organization in functional brain networks in the intermediate phase at multiple scales [57]. Using the Kuramoto model, power-law probability distributions have been found in a critical state and human brain functional systems, which are dynamically critical in an endogenous state [23]. The latest study reported the synchronization behavior on a large, weighted human connectome network under the homeostatic state. Further, it confirmed a power-law-tailed distribution of temporal duration of such synchronization behavior in the critical exponents [42]. The Kuramoto model is a convenient and valid tool for extracting the generic features of complex brain dynamics phenomena based on the parametric phase dynamics. It can unveil the synchrony strength among the brain regions by the coupling matrix and quantify the overall coherence by the Kuramoto order parameter. Phase transition only occurred at those critical dimensions, which represent the emergence of an asynchronous phase and a synchronous phase [36]. However, despite few applications in brain networks [23, 42, 54, 57], the potential of the Kuramoto model in neuroscience is vastly underestimated.

Oxytocin (OT), as a neuropeptide, can modulate neural activity and synchronization in the brain networks [58, 63], resulting in enhanced social adaptation and prosocial behaviors [8, 20, 33, 50]. In the early days, researchers focused on the effect of OT on specific brain regions, such as amygdala [24], temporoparietal junction (TPJ) [58]. With some in-depth studies on the connectivity analysis of brain networks, more attention has been shifted towards investigating the network level effects of OT. Wu et al. have found that OT significantly increases the functional connectivity between right TPJ and default attention network while decreases the connectivity between left TPJ and medial prefrontal network [58]. Schiller et al. have reported that OT reduced the occurrence and coverage of autonomous-processing related networks but increased the coverage of attention-related networks [26], implying that OT might reduce resources for the internal autonomous information process and allocate more resources to the external information process. The frontoparietal network

(FPN) is a brain network closely related to processing external information such as language and working memory. Our previous study has found that OT decreases the small-worldness of FPN and increases the average shortest path of the frontal nodes in FPN [63].

In contrast to FPN that is associated with external information processing, the default mode network (DMN) processes more internal information [35]. Many studies have shown that OT affects neural activity in DMN and its functional connectivity with other brain networks [19, 26, 58]. For example, it has been reported that OT reduces the functional connectivity between DMN nodes [5], reverses interactions between the DMN and the central executive network [26], and enhances the effective connectivity from the midline default network (posterior cingulate and precuneus) to the significant network [19]. Further investigations on a subnetwork of DMN, the frontal network as an upstream information processing center receiving inputs from downstream regions, have found that OT strengthens effective connectivity between brain cortex in the prefrontal and orbital prefrontal cortex [19], and changes the topography of the frontal areas and the interactions between the downstream areas such as the amygdala [40].

High levels of synchronization have been found within a brain subnetwork rather than between subnetworks [14], which is also known as enhanced within-network connectivity. It has been shown that oxytocin can decrease the clustering coefficients of the frontal nodes in the FPN network [63], reduce the functional connectivity between DMN nodes [5]. Although oxytocin effects on functional connectivity within specific networks are well studied, how oxytocin affects the synchronization between nodes within/between networks is largely unknown. Based on previous literature, we formulate the following three hypotheses: 1) OT changes the brain network topology such as DMN and FPN structures, which can be shown with community detection; 2) OT reduces the synchronization between the detected nodes in DMN but enhances synchronization in FPN, which can be shown with Kuramoto-based analysis; 3) OT increases the flexibility of DMN and FPN, which can be shown as increased variability of dynamical coupling patterns across time and subjects.

To validate our hypotheses, an fMRI study to investigate the OT effects on brain network dynamics is conducted. We apply the Kuramoto model dynamics framework to characterize the underlying neural synchronization in OT and PL groups. The framework consists of community detection in the network, Hilbert transform for phase information extraction, fitting coupling terms with interested communities in the Kuramoto model, and clustering the coupling terms. We demonstrate that the Kuramoto model, a tool to estimate the phase dynamics, has a great potential to unveil the effects of OT on brain network dynamics.

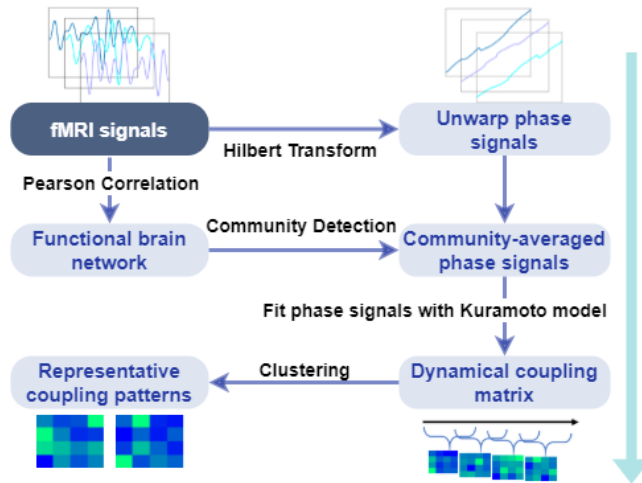


Figure 1: **Kuramoto model-based framework**

The framework is to characterize dynamical coupling in brain network.

## 2 Method

We propose a Kuramoto model-based framework to characterize neural synchronization and interactions between brain networks using fMRI data as shown in the flow diagram (**Figure 1**). Specifically, the framework includes the following analysis: 1) fMRI data preprocessing, 2) network detection and community detection, 3) perform Hilbert transformation to the fMRI signals to obtain the phase representation, 4) fit the Kuramoto model to fMRI data with sliding window to identify the coupling matrices of interested communities, 5) clustering analysis on the coupling matrices to obtain representative coupling patterns across time, 6) characterize and visualize the clustered coupling patterns.

### 2.1 Kuramoto model

For simplicity, we start from the simplest form of the Kuramoto model [28].

$$\dot{\theta}_i(t) = \omega_i + \frac{K}{N} \sum_{j=1}^{j=N} \Gamma(\theta_j - \theta_i) \quad (1)$$

In the above form,  $\omega_i$  represents the natural frequency of the  $i^{th}$  oscillator. The function  $\Gamma$  is the response function of the phase difference between two oscillators. The function  $\Gamma(\phi)$  illustrates the time average phase response of voltage difference. Under some experimental and theoretical settings, the expression of  $\Gamma(\phi)$  could be specified biologically, leading to an accurate calculation [12]. In Chapter 8 of Ermentrout’s book, it has been shown that the Kuramoto

model naturally arises from several assumptions of the system. These assumptions include weak coupling and asymptotic phase function approximation of the oscillator's state [14].

In our study, we choose  $\Gamma(\phi)$  to be  $\sin \phi$ . The simplified sin interaction function has been applied to mesoscale brain network research and reveal many critical brain functional mechanisms [18,22,29]. The successful application of the simplified coupling function suggests that the sinusoidal form coupling function can capture interregional dynamics. We now rewrite Eq(1) as follow.

$$\dot{\theta}_i(t) = \omega_i + \frac{K}{N} \sum_{j=1}^{j=N} \sin(\theta_j - \theta_i) \quad (2)$$

To go one step further, we consider heterogeneous connections. It is well-recognized that the coupling strength is not identical across pairs of interactions. The coupling could be excitatory or inhibitory, depending on the value of coupling strength. So we write  $K$  (scalar) as  $K_{ij}$  (now  $K$  becomes a matrix), and the equation becomes:

$$\dot{\theta}_i(t) = \omega_i + \frac{1}{N} \sum_{j=1}^{j=N} K_{ij} \sin(\theta_j - \theta_i) \quad (3)$$

We use Eq(3) in our study because of its simplicity and ability to capture critical dynamics, although there are other variants of Eq(3), which may provide a better approximation [18].

## 2.2 Hilbert transform to obtain phase dynamics

After the signals in ROI are extracted, Hilbert transform can be used to obtain phase signals. Many previous studies have adopted this approach to obtain the phase signal [25, 29]. If  $X(\omega)$  is the input signal and  $Y(\omega)$  is the output signal, we could express the Hilbert transform of  $X(\omega)$  in the frequency space:

$$Y(\omega) = X(\omega) * -i\text{sgn}(\omega) \quad (4)$$

Here  $X(\omega)$  is the Fourier transform of  $x(t)$ .  $\text{sgn}(\omega)$  is a sign function.  $-i$  can be written as  $e^{-i\frac{\pi}{2}}$ , which is a constant. If we expand  $x(t)$  to a Fourier series, we can see that every Fourier component is shifted by  $90^\circ$ . We could rewrite  $y(t)$  as:

$$y(t) = \Re\left(\sum_{n=-N}^{n=N} c_n * e^{i(\frac{2\pi}{T}nt \pm \frac{\pi}{2})}\right) \quad (5)$$

The following equations can provide insights about how to deduce phase signals using Hilbert transform:  $\tan(\theta) = \frac{\sin(\theta)}{\cos(\theta)} = \frac{\cos(\theta - \frac{\pi}{2})}{\cos(\theta)}$ ,  $\theta = \arctan(\frac{\cos(\theta - \frac{\pi}{2})}{\cos(\theta)})$ . For the filtered fMRI signal, the frequency band is narrow, suggesting a small number of frequency components [17]. So the phase of fMRI signal can be well approximated by:

$$\theta(t) = \arctan\left(\frac{H(x(t))}{x(t)}\right) \quad (6)$$

### 2.3 Order parameter

In statistical mechanics, we could define an order parameter to quantify the system's behavior during phase transition. The order parameter in the Kuramoto model is defined as:

$$R(t) = \left| \frac{1}{N} \sum_{n=1}^{n=N} e^{i\phi_n(t)} \right| \quad (7)$$

The motivation behind the definition of  $R(t)$  is intuitive. Imagine if all oscillators are in phase, then in the complex plane, each  $e^{i\phi_n(t)}$  will not cancel out but direct to the same direction. In this case,  $R(t)$  turns out to be 1. If all oscillators are out of phase,  $R(t)$  will approximate 0. Therefore, in oscillation models,  $R(t)$  is used to quantify the synchrony level within the system. The higher averaged  $R(t)$  indicates a higher synchrony level.

### 2.4 Model fitting to estimate dynamical coupling matrix

Here we introduce our method to fit the coupling strength  $k_{ij}$  between the node  $i$  and the node  $j$  with the following equation:

$$\dot{\theta}_i(t) = \omega_i + \frac{k_{ij}}{N} \sum_{j=1}^{j=N} \sin(\theta_j - \theta_i) \quad (8)$$

The phase signal  $\theta_i(t)$  and natural frequency  $\omega_i$  can be obtained by Hilbert transform and Fourier analysis, respectively. The phase signal  $\theta_i(t)$  is obtained by averaging over the detected community. The value of  $\omega_i$  is the frequency of the largest Fourier component.

By forward Euler method, we could write the following formula:

$$\left( \frac{\theta_i(t+1) - \theta_i(t)}{dt} - \omega_i \right) N = k_{ij} \sum_{j=1}^{j=N} \sin(\theta_j(t) - \theta_i(t)) \quad (9)$$

Let the left hand side  $\left( \frac{\theta_i(t+1) - \theta_i(t)}{dt} - \omega_i \right) N$  be  $A$  and the right hand side  $k_{ij} \sum_{j=1}^{j=N} \sin(\theta_j(t) - \theta_i(t))$  be  $k_{ij}B$ . Then we obtain  $\hat{k}_{ij}$  by optimizing the following loss function:

$$\hat{k}_{ij} = \underset{k_{ij}}{\operatorname{argmin}} \|A - k_{ij}B\|_F^2 \quad (10)$$

To obtain dynamic coupling term  $\hat{k}$ , we apply the above calculations in every sliding window. A sliding window length is set to be 56 seconds, and the overlap length is 10 seconds [47].

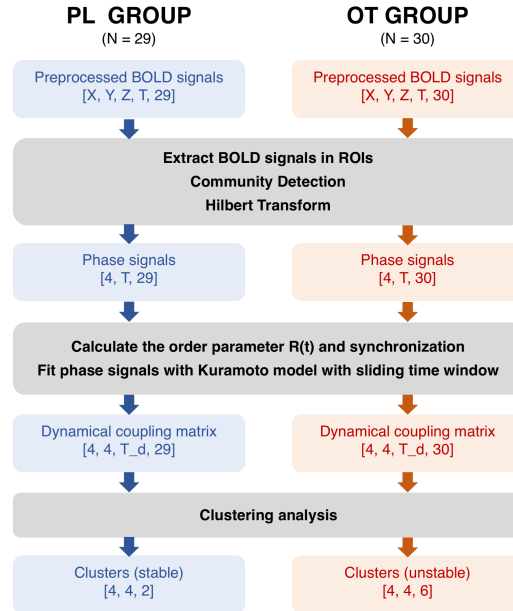


Figure 2: Data analysis pipeline

## 3 Experiments and Data Analyses

### 3.1 OT Administration and fMRI acquisition

We recruited 59 right-handed male college students (age ranging 19 ~ 26 years, and education ranging 13 ~ 18 years) via an online recruiting system in Beijing. All participants provided written consent, and the research protocol was approved by the institutional review board of Beijing Normal University. All participants completed a screening form and were included in the study only if they were confirmed that they did not have any major medical or mental illness, did not take drugs, did not drink and / or smoke every day. Before the experiment, participants were asked not to smoke or drink water (except water) for two hours. We used a double-blind placebo-controlled group design with participants randomly assigned to the oxytocin (OT) group or the placebo (PL) group. Each participant administered either 24 IU oxytocin or 24 IU placebo intranasally by three puffs of 8 IU per nostril. 45 minutes after administration, the participants have a 5-minute resting-state scan before any tasks. All images were acquired on a 3T Siemens Tim Trio scanner. More details of scanning parameters and fMRI preprocessing are shown in [58, 63].

### 3.2 Brain network community detection

In our study, we applied the community detection algorithm in both OT and PL groups. The group-level community is constructed using the virtual-typical-subject (VTS) approach [56], which used group-averaged functional connectivity matrices (obtained by Pearson correlation) to extract community patterns for the PL and the OT groups. Then we applied the Louvain heuristics algorithm with the structural resolution parameter  $\gamma = 1.9$ . Here,  $\gamma$  controls the modular size in the community detection. A higher  $\gamma$  value allows the algorithm to detect a community with a smaller size. Since it is an unsupervised algorithm, we iterate the algorithm 100 times to obtain a stable community structure with the highest Q value. Here, the Q value quantifies the modularity of corresponding networks.

### 3.3 Kuramoto model related analysis

Kuramoto model-based phase synchronization analysis in the detected community nodes is conducted to characterize the oxytocin effects on neural synchronization. We firstly apply the Hilbert transformation on fMRI data to obtain the phase signals. Then we average the phase signals over each of the 4 detected communities. We further calculate the temporal mean of the order parameter  $R(t)$  in these community-averaged signals. The temporal-averaged  $R(t)$  quantifies the synchronization level. To find oxytocin effects in altering network synchronization, we perform ranksum test to compare cross-community synchronizations between the PL and the OT groups.

To fit phase signals with the Kuramoto model, we take a community-averaged signal as the phase of one oscillator.  $N$  in Eq( 2) is set equal to 4, corresponding to the number of oscillators.  $\omega_i$  is obtained from averaging peak frequencies (of fMRI signal) over nodes within a community. The length of the sliding window is set to be 56 seconds with 10 seconds overlap [47]. There are 6 time windows in total. We run our fitting algorithm for each subject in every time window (See *Method* for details of the fitting algorithm). The details of the data analysis pipeline are summarized in **Figure 2**.

## 4 Results

### 4.1 OT effects on synchronization level

By community detection, we find 4 communities in each group. The highest Q value is 0.1510 for the PL group and 0.1477 for the OT group. We summarize our community detection results in **Table 1**. Our results find that both the PL and OT groups have two communities in FPN and DMN, but they involve different brain regions (see a full list of brain regions for the detected four communities in **Table 1**).

We then further compare the synchronization level (the mean of the order parameter  $R(t)$ ) in each community between two groups (**Figure 3**). The



Table 1: **The 4 detected communities and brain regions for OT and PL groups.**

Community	Shared nodes	Nodes in OT group	Nodes in PL group
<i>comm 1 / comm A</i> in <b>FPN</b>	Frontal Sup R		
	Frontal Mid R		
	Frontal Mid Orb R		
	Parietal Inf R		Frontal Mid L
	Angular L	Cingulum Post L	Frontal Mid Orb L
	Angular R	Cingulum Post R	Parietal Inf L
	Precuneus L		
	Precuneus R		
	Temporal Inf L		
Temporal Inf R			
<i>comm 2 / comm B</i> in <b>FPN</b>	Frontal Inf Oper L		Precentral L
	Frontal Inf Oper R	Frontal Mid L	Cingulum Mid R
	Frontal Inf Tri L	Frontal Inf Orb L	Parietal Sup R
	Frontal Inf Tri R	Parietal Inf L	SupraMarginal R
	SupraMarginal L		
<i>comm 3 / comm C</i> in <b>DMN</b>	Frontal Sup Orb L		
	Frontal Sup Orb R		
	Olfactory L	Amygdala L	
	Olfactory R,	Amygdala R,	Frontal Med Orb R
	Frontal Med Orb L	Hippocampus L	Cingulum Post L
	Rectus L	Hippocampus R	Cingulum Post R
	Rectus R	ParaHippocampal L	
	Temporal Pole Mid L	ParaHippocampal R	
Temporal Pole Mid R			
<i>comm 4 / comm D</i> in <b>DMN</b>	Frontal Sup L	Frontal Med Orb R	Frontal Inf Orb L
	Frontal Sup Medial L	Cingulum Ant R	Frontal Inf Orb R
	Cingulum Ant L	Caudate L	Frontal Sup Medial R
		Temporal Pole Sup L	Temporal Mid R

statistical results show significant differences in a community related to FPN ( $p = 0.0357, z = -2.0999$  with *ranksum* test on *comm 2* in PL and *comm B* in OT) and a community related to DMN ( $p = 0.0169, z = 2.3880$  with *ranksum* test on *comm 3* in PL and *comm C* in OT). Specifically, oxytocin increases synchronization in *comm B* in FPN but decreases *comm C* in DMN.

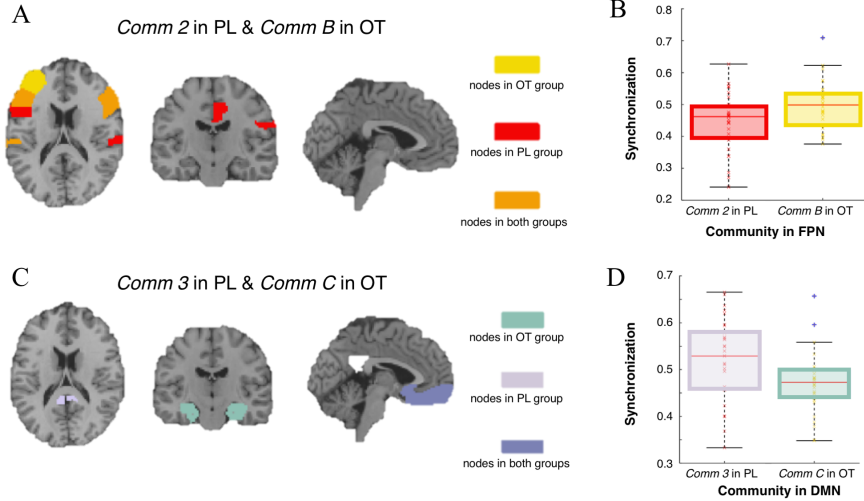


Figure 3: **Synchronization analysis.** (A) Visualization of detected community in FPN. The detected 4 nodes in *comm 2* for the PL group, 3 nodes in *comm B* for the OT group and 5 shared nodes in both groups are indicated with different colors. (B) Comparison of synchronization in community in FPN. The synchronization of the OT group is significantly higher than the PL group ( $p = 0.0357, z = -2.0999$ ). (C) Visualization of detected community in DMN. The detected 3 nodes in *comm 3* for the PL group, 6 nodes in *comm C* for the OT group and 9 shared nodes in both groups are indicated with different colors. (D) Comparison of synchronization in community in DMN. The synchronization of the OT group is significantly lower than the PL group ( $p = 0.0169, z = 2.3880$ ).

## 4.2 Variance of the coupling strength

In this section, we show our results in the analysis of the coupling strength's variance. In **Figure 4A**, we show the naming of communities and related coupling strengths.

We calculate the variance of  $k_{ij}(t)$  for each subject.  $t$  ranges from 1 to 6, representing 6 time windows. The only significant difference occurs between the variance of  $k_{43}$  and  $k_{DC}$  (See **Figure 4B**). The variance of  $k_{43}$  is higher than the variance of  $k_{DC}$  with  $p = 0.043, z = -2.0241$ . The upper plot in **Figure 4B** corresponds to the fitted  $k_{DC}$  in the PL group, and below corresponds to the

$k_{43}$  in the OT group. In Figure 4B, the red dot separates different subjects. There are 6 data points (correspond to 6 fitted  $k$ s in 6 time windows) between two neighboring red dots.

Other pairs of coupling strength do not show any significant difference in the variance or the mean.

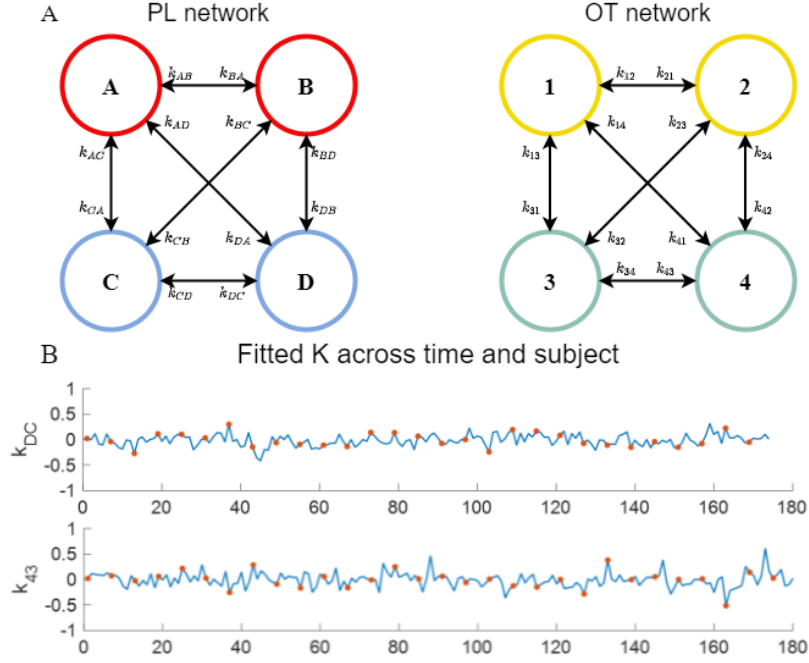


Figure 4: **Cross-community coupling.** (A)  $k_{ij}$  indicates the coupling strength between two communities in the PL group (left) and the OT group (right); (B) the coupling strengths,  $k_{DC}$  (upper) and  $k_{43}$  (bottom), across time and subjects. We concatenate the dynamical  $k$  from all subjects. The red dots indicate subjects.

### 4.3 Clustering of dynamical coupling patterns

Using Pearson correlation as a distance metric, we apply K-means clustering analysis on the dynamical coupling patterns across all subjects and all 6 sliding windows. In other words, there are  $29 \times 6$  coupling matrices in the PL group for clustering,  $30 \times 6$  coupling matrices in the OT group.

By maximizing silhouette value (evaluate the performance of clustering results), we obtain the optimal number of clusters. The optimal number of clusters is 2 for the PL group and 6 for the OT group. In **Figure 5**, we show obtained coupling patterns and the distance between clusters obtained from different trials, which evaluates the stability of clustering results.

In **Figure 5A**, we show 2 coupling patterns of corresponding averaged cluster centers. The clustering results for the PL group are stable. Through 200 iterations of the K-means algorithm (which randomly initializes the starting point), we find small correlation-based distances between the centers obtained in the first iteration and centers obtained in remain 199 iterations (See **Figure 5C**). In **Figure 5B**, we show 6 averaged cluster centers of the OT group. Different from the PL group, we find large distances between clusters in the OT group (See **Figure 5D**). The clustering results for the OT group are unstable.

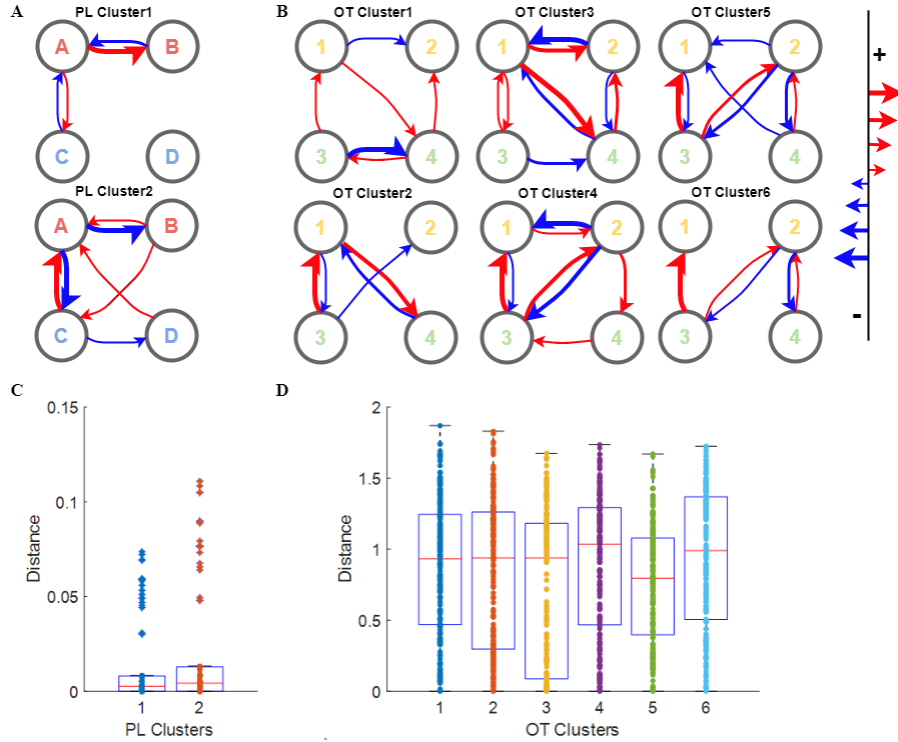


Figure 5: **The detected coupling patterns in clustering analysis.** (A) two clusters of coupling patterns in the PL group; (B) six clusters of coupling patterns in the OT group; (C) the distance of the detected clusters in the PL group with 200 iterations; (D) the distance of the detected clusters in the OT group with 200 iterations. The larger distance indicates a higher instability of the coupling pattern. Our results show that the detected dynamical coupling patterns in the PL group are more stable than those in the OT group; in return, coupling in the OT group has higher flexibility.

## 5 Discussion

### 5.1 Methodological Perspective

#### 5.1.1 Community Detection to Identify the Functional Structure

Recently, the modular topological structure identification in the network captured more attention in the neuroscience community. For instance, anatomical topology structure [13, 15] and functional topology structure [9] identification can differentiate the comparable groups. In this article, following our previous finding of the integration of DMN and FPN over the frontal region, we further apply the Louvain community detection algorithm to the functional connectivity matrix calculated by Pearson Correlation to identify the functional topology structure between OT and PL groups. We found that both PL and OT groups have two different communities in the FPN and the DMN (**Table 1**). The community structure in the PL group is well in line with the nodes in DMN and FPN, while OT communities do not necessarily match DMN and FPN structures, although there are many overlapped regions.

As an unsupervised machine learning approach, a considerable benefit of the Louvain community detection algorithm is that it does not require any prior knowledge about the community structure. The Louvain algorithm, therefore, has been widely applied to detect the community structure in the brain network [16]. However, without prior knowledge, the unsupervised nature might lead to challenges in explaining the detected communities and clarifying their links with brain function and behavior. Other approaches where prior knowledge can be combined with the independent component analysis have been adopted to detect brain networks [5, 59], resulting from a more robust detection of brain networks. Incorporating prior knowledge in community detection thus is one of the future directions in brain network science.

#### 5.1.2 Phase Synchronization with Kuramoto Model

The synchronization between individual neurons has been widely observed in previous studies [2, 7]. It has been mentioned that synchronization brings different sensory modalities together to produce a unified percept [14]. Synchronizations between brain regions were also observed and studied in the large-scale brain network [23, 60]. That is, neurons within the same brain region could be grouped. The synchronization between grouped signals reflects inter-regional information bindings. A technical review provides a detailed introduction to synchronization in the large-scale brain network [45].

Our study uses the order parameter  $R(t)$  in the Kuramoto model to measure the synchronization level in the large-scale brain network. As mentioned in *Method*, the definition of  $R(t)$  is straightforward. Therefore, the advantage of using  $R(t)$  as synchronization measure roots in the advantage of the phase signal. Compared to the raw fMRI signal, the phase signal is normalized, facilitating comparisons between subjects and regions (avoid baseline effects). Besides, the

phase signal represents the oscillator’s position in a circle, which captures the essence of the oscillation behavior.

The previous studies have found OT effects in reducing usage and duration of the autonomic processing-related microstates in favor of the attention-related microstates [53]. A higher synchronization level indicates longer functional maintenance of the corresponding network. Therefore, the OT-induced opposite effects on the autonomic processing-related microstates and the attention-related microstates are consistent with our findings.

### 5.1.3 Coupling Patterns among the Detected Communities

Intuitively, the connectivity matrix  $K$  reflects the collective neural activity among the brain network. A higher value indicates stronger coupling, which overcomes the dispersion of corresponding intrinsic frequencies to yield coherence, while a lower value denotes the asynchronous behavior [4, 52].

When we calculate the variance of coupling strength for each subject among 6 time windows, it shows a significant difference of the variance between  $k_{43}$  and  $k_{DC}$  (Shown in **Figure 4 B**). A higher value of temporal variance indicates a more dynamical connectivity pattern. The coupling strength  $k_{DC}$  in the OT group has a larger variance across time than the corresponding coupling strength  $k_{43}$  in the PL group.

Further, we perform K-means clustering on dynamical coupling strength matrices to obtain coupling patterns. The center of each cluster represents a coupling pattern. Notice the symmetric nature of two coupling patterns in the PL group, suggesting a potential balance of interactions. However, the clustering results of the OT group are not stable. The exact forms of cluster centers vary broadly from trial to trial. This variety confirms that OT may induce more flexible coupling patterns, in line with our findings in the temporal variance of coupling strength.

## 5.2 Neuroscience Perspective

### 5.2.1 OT exchanged the synchronization in FPN and DMN

Consistent with our hypothesis, we find the OT effect on synchronicity within the neural resting network. Specifically, OT reduces the synchronicity within DMN and increases the synchronicity within FPN. Once thought of only as a motor control network. However, there has been much recent evidence that FPN is essential to people’s ability to quickly and flexibly coordinate behavior [34], and these functions are more related to external information. In contrast, DMN involves the integration and refinement of existing knowledge and experience. Its activation increases when people engage in self-introspection [49, 62], which indicates internal information. Thus, this result may represent that people pay more attention to others (external information) and less attention to themselves, which may answer why OT can increase people’s cooperative behaviors [10, 61]—people will consider more about the behavior of others and how they should

interact with others, rather than pay more attention to their benefits. Many studies support this conclusion in some ways, such that OT can enhance the sensitivity of subjects to external cues such as aggression and pain [37,41,46,64].

### 5.2.2 OT increased variability of coupling strength in DMN

Previous studies have shown that OT can increase the responsiveness of humans and other species in both social and non-social domains [21], thereby improve their learning and social adaptation [43,65]. Here we examine the variance of the resting networks coupling under OT and PL groups. The result of increased variability confirms our second hypothesis that OT increases the flexibility of brain network coupling. This finding further indicates that OT can improve the sensitivity to external cues, which may help people and other species in social adaptation [44]. Therefore, we conducted cluster analysis on the coupling patterns between the brain networks of the subjects under the two treatments. We precisely find the effect of OT on the proliferation of coupling patterns. Specifically, OT increased the variance of coupling strength and produced more coupling patterns among the detected communities. This result may suggest that OT can increase the number of modulation strategies available to people.

One recent study on OT shows that OT can stabilize behavior through changing, a phenomenon known as allostasis [48]. Briefly, when a system is in a very elastic state, it is less likely to be destroyed. Our finding suggests that OT does increase instability between DMN and FPN (**Figure 5**), partially supporting the theory of higher instability with higher flexibility.

### 5.3 Limitations and Future Works

It is worthy of mentioning the challenges and limitations of our work. First, one central challenge in our research is that guaranteeing the fitted phase coupling matrix  $K$  could faithfully reflect the fundamental brain dynamics. When simulating the Kuramoto model, a strong coupling exists between two phase-locked oscillators. However, if we fit two phase-locked oscillators with the Kuramoto model, the fitted  $k$  might be small, which fails to reflect system dynamics. In our study, we overcome this challenge by first applying community detection to a correlation-based functional network. One oscillator’s signal is obtained by averaging phase signals over a detected community (high cohesion within an oscillator). This step guarantees that the synchronicity between our averaged-oscillators is low. Thus it could improve the authenticity of the fitted  $K$ . More advanced brain network community detection algorithms have been proposed and might contribute to brain network analysis. For example, the dynamic Plex Percolation Method, with its robustness to edge noise, can capture certain stereotypical dynamic community behaviors and track dynamic community organization [38]. By adding prior information, the evolutionary nonnegative matrix factorization method detects a more accurate dynamic community structure [32]. For identifying those with multi-layer networks functional community,

fusing nonnegative matrix factorization and topological structural information can explore more high-order information [31].

Validating the Kuramoto model at multiple temporal scales is an interesting future direction. Brain dynamics exist in multiple time scales. Due to the time resolution limitation of fMRI signals, our studies could only reveal large time scale dynamics. Complex, hierarchical, and high-resolution spatio-temporal dynamics of OT effects can not be accurately detected with fMRI. Other neuroimaging techniques with a finer time resolution should be incorporated and compared in our future study. For instance, an EEG study [53] explores the temporal stability of four archetypal EEG resting networks.

There are still some unexplained neural mechanisms underlying the statistical findings of oxytocin effects. For instance, the detected increasing or decreasing functional connectivity and the information flow among the resting-state networks. More physical-related dynamics methods (e.g., Hopf Oscillators, Quantum Harmonic Oscillators) with their interpretability might explain these physiological phenomena and drive neuroscience to a new era.

## Acknowledgement

This research was supported by National Natural Science Foundation of China (No. 62001205,U1736125), Guangdong Natural Science Foundation Joint Fund (No. 2019A1515111038),Guangdong natural science foundation(No.2021A1515012509), Shenzhen Key Laboratory of Smart Healthcare Engineering (ZDSYS20200811144003009). All authors declare no conflicts of interests.

## References

- [1] D. S. Bassett, P. Zurn, and J. I. Gold. On the nature and use of models in network neuroscience. *Nat. Rev. Neurosci*, 19(9):566–578, 2018.
- [2] M. V. Bennett and R. S. Zukin. Electrical coupling and neuronal synchronization in the mammalian brain. *Neuron*, 41(4):495–511, 2004.
- [3] C. Bick, M. Goodfellow, C. R. Laing, and E. A. Martens. Understanding the dynamics of biological and neural oscillator networks through exact mean-field reductions: a review. *The Journal of Mathematical Neuroscience*, 10:1–43, 2020.
- [4] M. Breakspear, S. Heitmann, and A. Daffertshofer. Generative models of cortical oscillations: neurobiological implications of the kuramoto model. *Frontiers in human neuroscience*, 4:190, 2010.
- [5] K. Brodmann, O. Gruber, and R. Goya-Maldonado. Intranasal oxytocin selectively modulates large-scale brain networks in humans. *Brain Connectivity*, pages 454–463, 2017.



- [6] J. Cabral, E. Hugues, O. Sporns, and G. Deco. Role of local network oscillations in resting-state functional connectivity. *Neuroimage*, 57(1):130–139, 2011.
- [7] M. Chiappalone, A. Vato, L. Berdondini, M. Koudelka-Hep, and S. Martinoia. Network dynamics and synchronous activity in cultured cortical neurons. *International journal of neural systems*, 17(02):87–103, 2007.
- [8] P. S. Churchland and P. Winkelman. Modulating social behavior with oxytocin: how does it work? what does it mean? *Horm. Behav.*, 61(3):392–399, 2012.
- [9] N. A. Crossley, A. Mechelli, P. E. Vértes, T. T. Winton-Brown, A. X. Patel, C. E. Ginestet, P. McGuire, and E. T. Bullmore. Cognitive relevance of the community structure of the human brain functional coactivation network. *Proceedings of the National Academy of Sciences*, 110(28):11583–11588, 2013.
- [10] C. K. De Dreu and M. E. Kret. Oxytocin conditions intergroup relations through upregulated in-group empathy, cooperation, conformity, and defense. *Biological psychiatry*, 79(3):165–173, 2016.
- [11] A. Delorme and S. Makeig. Eeglab: an open source toolbox for analysis of single-trial eeg dynamics including independent component analysis. *Journal of neuroscience methods*, 134(1):9–21, 2004.
- [12] R. Dodla and C. J. Wilson. Effect of phase response curve shape and synaptic driving force on synchronization of coupled neuronal oscillators. *Neural computation*, 29(7):1769–1814, 2017.
- [13] J. M. Duarte-Carvajalino, N. Jahanshad, C. Lenglet, K. L. McMahon, G. I. De Zubicaray, N. G. Martin, M. J. Wright, P. M. Thompson, and G. Sapiro. Hierarchical topological network analysis of anatomical human brain connectivity and differences related to sex and kinship. *Neuroimage*, 59(4):3784–3804, 2012.
- [14] G. B. Ermentrout and D. H. Terman. *Mathematical foundations of neuroscience*, volume 35. Springer Science & Business Media, 2010.
- [15] Y. Fan, F. Shi, J. K. Smith, W. Lin, J. H. Gilmore, and D. Shen. Brain anatomical networks in early human brain development. *Neuroimage*, 54(3):1862–1871, 2011.
- [16] J. O. Garcia, A. Ashourvan, S. Muldoon, J. M. Vettel, and D. S. Bassett. Applications of community detection techniques to brain graphs: Algorithmic considerations and implications for neural function. *Proceedings of the IEEE*, 106(5):846–867, 2018.

- [17] S. R. Gohel and B. B. Biswal. Functional integration between brain regions at rest occurs in multiple-frequency bands. *Brain connectivity*, 5(1):23–34, 2015.
- [18] P. J. Hellyer, M. Shanahan, G. Scott, R. J. Wise, D. J. Sharp, and R. Leech. The control of global brain dynamics: opposing actions of frontoparietal control and default mode networks on attention. *Journal of Neuroscience*, 34(2):451–461, 2014.
- [19] X. Jiang, X. Ma, Y. Geng, Z. Zhao, and K. M. Kendrick. Intrinsic, dynamic and effective connectivity among large-scale brain networks modulated by oxytocin. *NeuroImage*, 2020.
- [20] C. Jones, I. Barrera, S. Brothers, R. Ring, and C. Wahlestedt. Oxytocin and social functioning. *DIALOGUES CLIN NEURO*, 19(2):193, 2017.
- [21] G. E. Kapetaniou, M. A. Reinhard, P. Christian, A. Jobst, P. N. Tobler, F. Padberg, and A. Soutschek. The role of oxytocin in delay of gratification and flexibility in non-social decision making. *Elife*, 10:e61844, 2021.
- [22] A. Kashyap and S. Keilholz. Dynamic properties of simulated brain network models and empirical resting-state data. *Network Neuroscience*, 3(2):405–426, 2019.
- [23] M. G. Kitzbichler, M. L. Smith, S. R. Christensen, and E. Bullmore. Broad-band criticality of human brain network synchronization. *PLoS Comput Biol*, 5(3):e1000314, 2009.
- [24] S. Koch, M. V. Zuiden, L. Nawijn, J. L. Frijling, D. J. Veltman, and M. Olf. Intranasal oxytocin normalizes amygdala functional connectivity in posttraumatic stress disorder. *Neuropsychopharmacology*, 41(8):2041–2051, 2016.
- [25] M. L. Kringelbach, J. Cruzat, J. Cabral, G. M. Knudsen, R. Carhart-Harris, P. C. Whybrow, N. K. Logothetis, and G. Deco. Dynamic coupling of whole-brain neuronal and neurotransmitter systems. *Proceedings of the National Academy of Sciences*, 117(17):9566–9576, 2020.
- [26] J. Kumar, S. J. Iwabuchi, B. A. Vllm, and L. Palaniyappan. Oxytocin modulates the effective connectivity between the precuneus and the dorso-lateral prefrontal cortex. *European Archives of Psychiatry and Clinical Neuroscience*, 270(9), 2019.
- [27] Y. Kuramoto. Cooperative dynamics of oscillator communitya study based on lattice of rings. *Progress of Theoretical Physics Supplement*, 79:223–240, 1984.
- [28] Y. Kuramoto. *Chemical oscillations, waves, and turbulence*. Courier Corporation, 2003.

- [29] W. H. Lee and S. Frangou. Linking functional connectivity and dynamic properties of resting-state networks. *Scientific reports*, 7(1):1–10, 2017.
- [30] Q. Liu, S. Farahibozorg, C. Porcaro, N. Wenderoth, and D. Mantini. Detecting large-scale networks in the human brain using high-density electroencephalography. *Human Brain Mapping*, 38(9):4631–4643, 2017.
- [31] C. Ma, Q. Lin, Y. Lin, and X. Ma. Identification of multi-layer networks community by fusing nonnegative matrix factorization and topological structural information. *Knowledge-Based Systems*, 213:106666, 2021.
- [32] X. Ma and D. Dong. Evolutionary nonnegative matrix factorization algorithms for community detection in dynamic networks. *IEEE transactions on knowledge and data engineering*, 29(5):1045–1058, 2017.
- [33] Y. Ma, S. Shamay-Tsoory, S. Han, and C. F. Zink. Oxytocin and social adaptation: insights from neuroimaging studies of healthy and clinical populations. *Trends Cogn. Sci.*, 20(2):133–145, 2016.
- [34] S. Marek and N. U. Dosenbach. The frontoparietal network: function, electrophysiology, and importance of individual precision mapping. *Dialogues in clinical neuroscience*, 20(2):133, 2018.
- [35] M. Marino, Q. Liu, J. Samogin, F. Tecchio, C. Cottone, D. Mantini, and C. Porcaro. Neuronal dynamics enable the functional differentiation of resting state networks in the human brain. *Human brain mapping*, 40(5):1445–1457, 2019.
- [36] H. Markram, E. Muller, S. Ramaswamy, M. W. Reimann, M. Abdellah, C. A. Sanchez, A. Ailamaki, L. Alonso-Nanclares, N. Antille, S. Arsever, et al. Reconstruction and simulation of neocortical microcircuitry. *Cell*, 163(2):456–492, 2015.
- [37] N. Marsh, A. A. Marsh, M. R. Lee, and R. Hurlemann. Oxytocin and the neurobiology of prosocial behavior. *The Neuroscientist*, page 1073858420960111, 2020.
- [38] L.-E. Martinet, M. Kramer, W. Viles, L. Perkins, E. Spencer, C. Chu, S. Cash, and E. Kolaczyk. Robust dynamic community detection with applications to human brain functional networks. *Nature communications*, 11(1):1–13, 2020.
- [39] F. S. Matias, L. L. Gollo, P. V. Carelli, S. L. Bressler, M. Copelli, and C. R. Mirasso. Modeling positive granger causality and negative phase lag between cortical areas. *NeuroImage*, 99:411–418, 2014.
- [40] C. Morawetz, S. Bode, J. Baudewig, and H. R. Heekeren. Effective amygdala-prefrontal connectivity predicts individual differences in successful emotion regulation. *Soc. Cogn. Affect. Neurosci.*, 12(4):569–585, 2017.

- [41] R. Ne’eman, N. Perach-Barzilay, M. Fischer-Shofty, A. Atias, and S. Shamay-Tsoory. Intranasal administration of oxytocin increases human aggressive behavior. *Hormones and behavior*, 80:125–131, 2016.
- [42] G. Ódor and J. Kelling. Critical synchronization dynamics of the kuramoto model on connectome and small world graphs. *Scientific reports*, 9(1):1–10, 2019.
- [43] D. E. Olazábal and N. Y. Sandberg. Variation in the density of oxytocin receptors in the brain as mechanism of adaptation to specific social and reproductive strategies. *General and comparative endocrinology*, 286:113337, 2020.
- [44] D. E. Olazabal and L. J. Young. Species and individual differences in juvenile female alloparental care are associated with oxytocin receptor density in the striatum and the lateral septum. *Hormones and behavior*, 49(5):681–687, 2006.
- [45] G. C. O’Neill, P. Tewarie, D. Vidaurre, L. Liuzzi, M. W. Woolrich, and M. J. Brookes. Dynamics of large-scale electrophysiological networks: A technical review. *Neuroimage*, 180:559–576, 2018.
- [46] M. Pfundmair, C. Zwarg, M. Paulus, and A. Rimpel. Oxytocin promotes attention to social cues regardless of group membership. *Hormones and behavior*, 90:136–140, 2017.
- [47] M. G. Preti, T. A. Bolton, and D. Van De Ville. The dynamic functional connectome: State-of-the-art and perspectives. *Neuroimage*, 160:41–54, 2017.
- [48] D. S. Quintana and A. J. Guastella. An allostatic theory of oxytocin. *Trends in cognitive sciences*, 2020.
- [49] M. E. Raichle. The brain’s default mode network. *Annual review of neuroscience*, 38:433–447, 2015.
- [50] H. E. Ross, C. D. Cole, Y. Smith, I. D. Neumann, R. Landgraf, A. Z. Murphy, and L. J. Young. Characterization of the oxytocin system regulating affiliative behavior in female prairie voles. *Neuroscience*, 162(4):892–903, 2009.
- [51] J. Samogin, Q. Liu, M. Marino, N. Wenderoth, and D. Mantini. Shared and connection-specific intrinsic interactions in the default mode network. *Neuroimage*, 200:474–481, 2019.
- [52] L. M. Sanchez-Rodriguez, Y. Iturria-Medina, P. Mouches, and R. C. Sotero. Detecting brain network communities: considering the role of information flow and its different temporal scales. *NeuroImage*, 225:117431, 2021.

- [53] B. Schiller, T. Koenig, and M. Heinrichs. Oxytocin modulates the temporal dynamics of resting eeg networks. *Scientific reports*, 9(1):1–9, 2019.
- [54] R. Schmidt, K. J. LaFleur, M. A. de Reus, L. H. van den Berg, and M. P. van den Heuvel. Kuramoto model simulation of neural hubs and dynamic synchrony in the human cerebral connectome. *BMC neuroscience*, 16(1):1–13, 2015.
- [55] O. Sporns. The human connectome: a complex network. *Annals of the new York Academy of Sciences*, 1224(1):109–125, 2011.
- [56] F. Taya, J. de Souza, N. V. Thakor, and A. Bezerianos. Comparison method for community detection on brain networks from neuroimaging data. *Appl. Netw. Sci.*, 1(1):8, 2016.
- [57] P. Villegas, P. Moretti, and M. A. Munoz. Frustrated hierarchical synchronization and emergent complexity in the human connectome network. *Scientific reports*, 4(1):1–7, 2014.
- [58] H. Wu, C. Feng, X. Lu, X. Liu, and Q. Liu. Oxytocin effects on the resting-state mentalizing brain network. *Brain Imaging Behav*, pages 1–12, 2020.
- [59] F. Xin, F. Zhou, X. Zhou, X. Ma, Y. Geng, W. Zhao, S. Yao, D. Dong, B. B. Biswal, K. M. Kendrick, et al. Oxytocin modulates the intrinsic dynamics between attention-related large-scale networks. *Cerebral Cortex*, 31(3):1848–1860, 2021.
- [60] T. Yamanishi, J.-Q. Liu, and H. Nishimura. Modeling fluctuations in default-mode brain network using a spiking neural network. *International journal of neural systems*, 22(04):1250016, 2012.
- [61] S. Yang, Q. Xu, and P. Li. Oxytocin modulates responsibility attribution and hypothetical resource allocation during cooperation. *Psychoneuroendocrinology*, 114:104597, 2020.
- [62] Y. Yeshurun, M. Nguyen, and U. Hasson. The default mode network: where the idiosyncratic self meets the shared social world. *Nature Reviews Neuroscience*, pages 1–12, 2021.
- [63] S. Zheng, D. Punia, H. Wu, and Q. Liu. Graph theoretic analysis reveals intranasal oxytocin induced network changes over frontal regions. *Neuroscience*, 459:153–165, 2021.
- [64] R. Zhu, C. Liu, T. Li, Z. Xu, B. Fung, C. Feng, H. Wu, Y. Luo, and L. Wang. Intranasal oxytocin reduces reactive aggression in men but not in women: A computational approach. *Psychoneuroendocrinology*, 108:172–181, 2019.
- [65] Q. Zhuang, S. Zhu, X. Yang, X. Zhou, X. Xu, Z. Chen, C. Lan, W. Zhao, B. Becker, S. Yao, et al. Oxytocin-induced facilitation of learning in a probabilistic task is associated with reduced feedback-and error-related negativity potentials. *Journal of Psychopharmacology*, page 0269881120972347, 2020.